2nd International Conference on the Material Point Method for Modelling Soil-Water-Structure Interaction

Anura3D
MPM Research Community

Paper number: mpm2019.02
www.anura3d.com
www.mpm2019.eu

Second-order convected particle domain interpolation (CPDI2) with triangular grid elements and triangular particle domains

Vibhav, Bisht[1,*], Rodrigo, Salgado[1]
[1]School of Civil Engineering, Purdue University, West Lafayette, USA

[*] E-mail: bisht.vibhav@gmail.com

ABSTRACT

Several variants of the material point method (MPM) have been developed that attempt to improve upon the original method. One particularly attractive variant of MPM is the convected particle domain interpolation (CPDI2) method, which offers several advantages: it does not exhibit cell-crossing instability nor exhibits extension instability; precisely tracks particle domains; accurately evaluates surface integrals, such as tractions; and uses shape functions that are a partition of unity. In theory, the CPDI2 method allows efficient interpolation of convex polygonal particle domains in structured and unstructured meshes. This flexibility can be utilized for construction of triangular particle domains that can conform to complex geometries and cross-patched triangular meshes, which are known to mitigate volumetric locking. This paper formulates CPDI2 shape functions for quadrilateral and triangular particle domains with quadrilateral and triangular grid elements and verifies their accuracy by comparison against analytical and benchmark solutions.

KEY WORDS: Material point method; Convected particle domain interpolation; Verification.

INTRODUCTION

The material point method (MPM) (Sulsky, Chen and Schreyer, 1994; Sulsky, Zhou and Schreyer, 1995) is a particle-based method well-suited for simulating large deformation problems with complex history-dependent materials. There are several variants of MPM (Bardenhagen and Kober, 2004; Steffen, Kirby and Berzins, 2008; Sadeghirad, Brannon and Burghardt, 2011; Zhang, Ma and Giguere, 2011; Sadeghirad, Brannon and Guilkey, 2013; Woo and Salgado, 2018), each resulting from an attempt to improve upon specific method deficiencies. Most of these deficiencies arise because the shape functions used in these methods have low-order (C^0) continuity and/or do not provide the means for efficient evaluation of integrals (such as internal and external forces) when material point domains are present across element boundaries. One promising variant that tackles these deficiencies is the convected particle domain interpolation (CPDI2) method (Sadeghirad, Brannon and Burghardt, 2011; Sadeghirad, Brannon and Guilkey, 2013), in which the shape functions are constructed to be an interpolant of values defined at corners of a particle domain. In CPDI2, the shape function $\overline{S^{IP}}$ for node I of the grid and material point P is given by:

$$\overline{S^{IP}}(\mathbf{x}) = \frac{1}{V^P}\sum_{\alpha}\left(\int_{\Omega^P} N_\alpha^P(\mathbf{x})\,\mathrm{d}\Omega\right) S^I(\mathbf{x}_\alpha) \quad : \mathbf{x} \in \Omega^P \tag{1}$$

where $\mathbf{x}$ is the co-ordinate vector, V^P is the volume of particle P, N_α^P is the standard finite element (FE) tent shape function defined within the particle domain as if it were an element, S^I is the standard FE shape function for node I (calculated in Equation (1) at corner α of particle P), and the summation is carried out over all corners α of the particle domain Ω^P.

By defining the shape functions as shown in Equation (1), the CPDI2 method allows efficient evaluation of integrals over deformed particle domains crossing element boundaries and hence permits tracking of particle domains with high precision. This resolves several shortcomings present in the original MPM method and several of its variants, such as cell-crossing instability (Bardenhagen and Kober, 2004; Steffen, Kirby and Berzins, 2008), extension instability (Sadeghirad, Brannon and Burghardt, 2011), inaccuracies due to the presence of gaps and overlaps (Kamojjala *et al.*, 2015), and inaccurate evaluation of surface integrals (Nairn and Guilkey, 2015).

Despite these advantages, the recent development of CPDI2 has precluded extensive development and testing of the method. Thus, although CPDI2 provides flexibility in choosing the shapes of the grid elements and particle domains, only formulations for 4-noded quadrilateral particle domains (Q^P4) with 4-noded quadrilateral grid elements (Q^E4) have been extensively used.
In this paper, CPDI2 shape functions under plane strain conditions for 3-noded triangular particle domains (T^P3) are formulated, as these excel at tessellating complicated geometries. In addition, 3-noded triangular grid elements (T^E3) arranged in a cross-patched configuration, known to mitigate volumetric locking, are utilized in conjunction with Q^P4 domains. The performance of these particle domain and mesh configurations are assessed by comparison against a benchmark solution and the analytical solution of the plane strain expansion of a linear-elastic cylinder under internal pressure.

CONVECTED PARTICLE DOMAIN INTERPOLATION (CPDI2)

Shape Functions and their Derivatives

In this section, the shape functions and their derivatives under plane strain conditions for quadrilateral and triangular particle domains are presented. The construction of CPDI2 shape functions (Equation (1)) can be divided into two parts: computation of $\int_{\Omega^P} N_\alpha^P(\mathbf{x})\mathrm{d}\Omega$ and interpolation of the computed values using standard FE shape functions $S^I(\mathbf{x}_\alpha)$. The evaluation of $\int_{\Omega^P} N_\alpha^P(\mathbf{x})\mathrm{d}\Omega$ is dependent only on the shape of the particle domain. The computation of $S^I(\mathbf{x}_\alpha)$ is dependent only on the background elements used for computation, i.e., for a T^E3 or Q^E4 element, $S^I(\mathbf{x}_\alpha)$ would simply be the value of the corresponding FE shape function for a T^E3 or Q^E4 element at position $\mathbf{x}_\alpha$. For a Q^P4 domain, the shape functions and their derivatives (given in [5]) are:

$$\begin{aligned}
\bar{S}^{IP} &= \frac{1}{24V^P}\left\{(1-a-b)S^I\left(\mathbf{x}_1^P\right)+(1-a+b)S^I\left(\mathbf{x}_2^P\right)+(1+a+b)S^I\left(\mathbf{x}_3^P\right)+(1+a-b)S^I\left(\mathbf{x}_4^P\right)\right\} \\
\nabla\bar{S}^{IP} &= \frac{1}{2V^P}\left\{S^I\left(\mathbf{x}_1^P\right)\begin{bmatrix} y_2^P-y_4^P \\ x_4^P-x_2^P\end{bmatrix}+S^I\left(\mathbf{x}_2^P\right)\begin{bmatrix} y_3^P-y_1^P \\ x_1^P-x_3^P\end{bmatrix}+S^I\left(\mathbf{x}_3^P\right)\begin{bmatrix} y_4^P-y_2^P \\ x_2^P-x_4^P\end{bmatrix}+S^I\left(\mathbf{x}_4^P\right)\begin{bmatrix} y_1^P-y_3^P \\ x_3^P-x_1^P\end{bmatrix}\right\}
\end{aligned} \tag{2}$$

where $\mathbf{x}_{1-4}^P$ are the co-ordinate vectors of the four corners of the domain of particle *P* and:

$$\begin{aligned}
a &= (x_4^P-x_1^P)(y_2^P-y_3^P)-(x_2^P-x_3^P)(y_4^P-y_1^P) \\
b &= (x_3^P-x_4^P)(y_1^P-y_2^P)-(x_1^P-x_2^P)(y_3^P-y_4^P)
\end{aligned} \tag{3}$$

For a T^P3 domain, the shape functions and their derivates are:

$$\begin{aligned}
\bar{S}^{IP} &= \frac{1}{3}\left\{S^I\left(\mathbf{x}_1^P\right)+S^I\left(\mathbf{x}_2^P\right)+S^I\left(\mathbf{x}_3^P\right)\right\} \\
\nabla\bar{S}^{IP} &= \frac{1}{2V^P}\left\{S^I\left(\mathbf{x}_1^P\right)\begin{bmatrix} y_2^P-y_3^P \\ x_3^P-x_2^P\end{bmatrix}+S^I\left(\mathbf{x}_2^P\right)\begin{bmatrix} y_3^P-y_1^P \\ x_1^P-x_3^P\end{bmatrix}+S^I\left(\mathbf{x}_3^P\right)\begin{bmatrix} y_1^P-y_2^P \\ x_2^P-x_1^P\end{bmatrix}\right\}
\end{aligned} \tag{4}$$

Traction Boundary Conditions

CPDI2 methods can be used to accurately integrate over the deformed surface of the object (Nairn and Guilkey, 2015). Assuming the traction vector **T** to be constant over the deformed edge, the traction forces $\mathbf{f}_T$ under plane-strain conditions can be computed to be:

$$\mathbf{f}_T^I = \frac{1}{2}\mathbf{T}L_{\text{Edge}}\left(S^I(\mathbf{x}_{\alpha 1})+S^I(\mathbf{x}_{\alpha 2})\right) \tag{5}$$

where L_{Edge} is the length of the deformed edge on which the traction is specified and $\mathbf{x}_{\alpha 1}$ and $\mathbf{x}_{\alpha 2}$ are the co-ordinates for the two corners of that edge.

SIMULATIONS

Two simulations are performed for verifying Equations (2)-(5) using an explicit solver with the update-stress-last algorithm (Bardenhagen, 2002). The first example is based on the method of manufactured solutions (MMS). In MMS, the displacement field is assumed *a priori*. The external forces required for these displacements to be in effect are determined analytically and applied as external forces in the simulation. The displacements arising due to the application of these external forces are computed in the simulation and compared against the displacement field that was assumed *a priori*. In the second example, a linear-elastic cylinder is radially loaded under plane-strain conditions. The analytical solution for this problem is known (Timoshenko and Goodier, 1951).

Axis-aligned Displacement of a Unit Square

The following displacement field **u** is assumed in a unit square:

$$\begin{aligned} u_x &= A\sin\left(2\pi X\right)\sin\left(C\pi t\right) \\ u_y &= A\sin\left(2\pi Y\right)\sin\left(C\pi t+\pi\right) \end{aligned} \tag{6}$$

where X and Y are co-ordinates in the reference configuration, A is the maximum amplitude of displacement ($A=0.05$), $C=\sqrt{E/\rho_0}$ where E is the Young's modulus ($E=1\times10^7 Pa$) and ρ_0 is the initial density ($\rho_0=1000kg/m^3$), and t is the time. The material is Neo-Hookean with Poisson's ratio $\nu=0.3$. The time steps for the simulations are taken as $\Delta t=0.4h/C$, where h is the cell spacing. Details pertaining to the corresponding external forces and their derivation can be found in Sadeghirad et al. (2011). Simulations are performed for 4 different grid resolutions – 8 × 8, 16 × 16, 32 × 32, 64 × 64, with 2 particles per cell in each direction using T^P3 domains with Q^E4 elements and 1 particle per cell using Q^P4 domains with T^E3 elements arranged in a cross-patched configuration. A sketch of the initial discretization for an 8 × 8 grid resolution is shown in Figure 1.

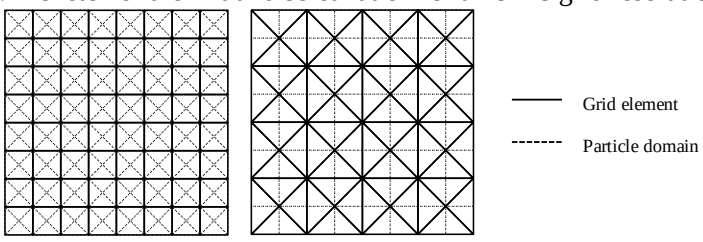

Figure 1 Initial discretization for the simulation of an axis-aligned displacement of a unit square using: (a) triangular particle domains with quadrilateral grid elements and (b) quadrilateral particle domains with triangular grid elements in a cross-patched configuration

The error norm for the example is defined as:

$$\text{Err}=\frac{\sqrt{\sum_{i=1}^{N_t}\sum_{P=1}^{N_P}\left\|\mathbf{u}^{\text{app}}(\mathbf{x}_P,t_i)-\mathbf{u}^{\text{exact}}(\mathbf{x}_P,t_i)\right\|^2}}{N_t\times N_P} \tag{7}$$

where $\mathbf{u}^{\text{app}}$ are the displacements computed from the simulations, $\mathbf{u}^{\text{exact}}$ are the displacements assumed *a priori*, and N_t and N_P are the number of time steps and number of particles, respectively. The error norms are evaluated at t = 0.02 s (one full period of oscillation). The convergence curves for the 4 grid resolutions considered in this example are shown in Figure 2. The results show that the error norms and convergence rate for the particle domain and grid element combinations considered are of the same order.

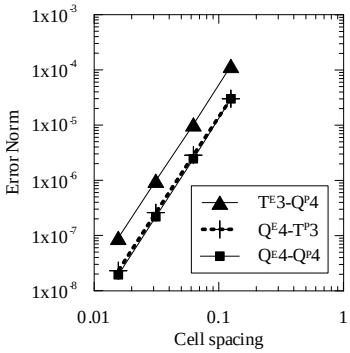

Figure 2 Convergence curves for the axis-aligned displacement in a unit square problem using CPDI2 with various particle domain and grid element shapes

Expansion of a Linear-Elastic Cylinder under Internal Pressure

A linear elastic cylinder with material properties $E = 100\,\text{kPa}$ and $\nu = 0.2$ is internally loaded with a radial pressure $p = 1\,\text{kPa}$ in plane strain. The pressure p has been applied using traction boundaries (Equation (5)). On the outer surface, standard viscous boundaries are specified to prevent reflected waves from affecting the solution. The forces required for damping the oncoming waves have been applied as tractions on the edges of particles present adjacent to the standard viscous boundary (see Shen & Chen 2005; Bisht & Salgado 2018). A sketch of the problem is shown in Figure 3. Only a quarter-sketch is shown, for the problem is symmetric.

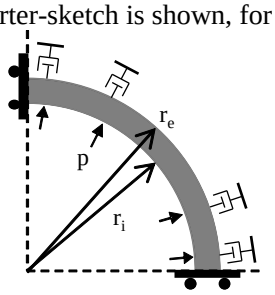

Figure 3 Sketch of a linear-elastic cylinder subject to an internal pressure

The analytical circumferential stress σ_θ for this problem is given by:

$$\boldsymbol{\sigma_\theta}(r) = p\frac{r_i^2}{r_e^2 - r_i^2}\left(1 + \frac{r_e^2}{r^2}\right) \tag{8}$$

where r_i ($r_i = 4\,\text{m}$) and r_e ($r_e = 9\,\text{m}$) are the internal and external radii respectively.

Discretization of both the body and space is shown in Figure 4. The body is discretized with Q^P4 particle domains whose maximum dimensions increase radially from 0.5 m to 0.7 m. The domain is discretized using T^E3 elements arranged in a cross-patched configuration with base = 1.0 m and height = 0.5 m.

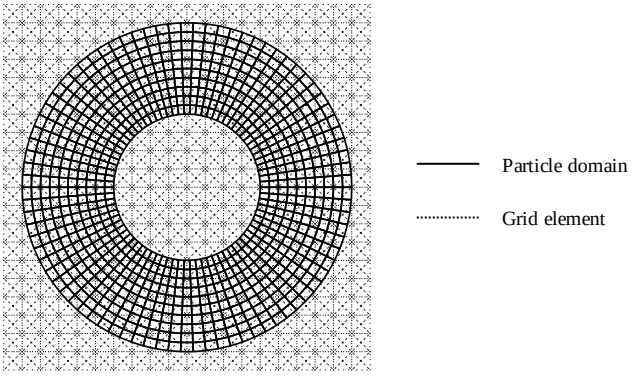

Figure 4 Discretization of a linear elastic cylinder using quadrilateral particle domains and triangular elements arranged in a cross-patched configuration

A contour plot of the circumferential stress is shown in Figure 5. It can be seen that the circumferential stress

decreases radially, in accordance with the analytical solution. The average error in the circumferential stress is < 6%, which decreases as the discretization is made finer (results not shown). The results for the circumferential stress are similar using other configurations of particle domain and grid element shapes specified in this study, but are not shown due to space constraints.

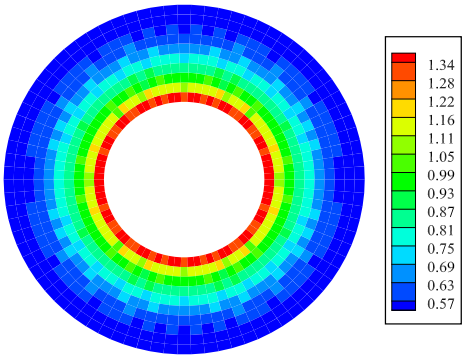

Figure 5 Contour plot of the circumferential stress for a linear-elastic cylinder subject to internal pressure

CONCLUSION

The CPDI2 method is an attractive variant to MPM, which resolves many deficiencies present in the original method. However, its recent conception has precluded extensive development and testing. The CPDI2 method provides flexibility in choosing the shapes of the particle domains and grid elements. In this paper, this flexibility is utilized for the construction of shape functions for CPDI2 particles with triangular domains and triangular grid elements in a cross-patched arrangement in plane strain. These shape functions have been verified by comparison against a benchmark MMS solution and the analytical solution of a known problem (internal loading of a hollow cylinder).

REFERENCES

Bardenhagen SG. (2002). Energy conservation error in the material point method for solid mechanics. *Journal of Computational Physics*. 180(1): 383–403.
Bardenhagen SG and Kober EM. (2004). The generalized interpolation material point method. *Computer Modeling in Engineering & Sciences*. 5(6): 477–496.
Bisht V and Salgado R. (2018). Local transmitting boundaries for the generalized interpolation material point method. *International Journal for Numerical Methods in Engineering*. 114(11): 1228–1244.
Kamojjala K, Brannon R, Sadeghirad A and Guilkey J. (2015). Verification tests in solid mechanics. *Engineering with Computers*. 31(2): 193–213.
Nairn JA and Guilkey JE. (2015). Axisymmetric form of the generalized interpolation material point method. *International Journal for Numerical Methods in Engineering*. 101(2): 127–147.
Sadeghirad A, Brannon RM and Burghardt J. (2011). A convected particle domain interpolation technique to extend applicability of the material point method for problems involving massive deformations. *International Journal for Numerical Methods in Engineering*. 86(12): 1435–1456.
Sadeghirad A, Brannon RM and Guilkey JE. (2013) Second-order convected particle domain interpolation (CPDI2) with enrichment for weak discontinuities at material interfaces. *International Journal for Numerical Methods in Engineering*. 95(11): 928–952.
Shen L and Chen Z. (2005). A silent boundary scheme with the material point method for dynamic analyses. *Computer Modeling in Engineering and Sciences*. 7(3): 305–320.
Steffen M, Kirby RM and Berzins M. (2008). Analysis and reduction of quadrature errors in the material point method (MPM),.*International Journal for Numerical Methods in Engineering*. 76(6): 922–948.
Sulsky D, Chen Z and Schreyer HL. (1994). A particle method for history-dependent materials. *Computer Methods in Applied Mechanics and Engineering*. 118(1–2): 179–196.
Sulsky D, Zhou SJ and Schreyer HL. (1995). Application of a particle-in-cell method to solid mechanics. *Computer Physics Communications*. 87(1–2): 236–252.
Timoshenko S and Goodier J. (1951). *Theory of elasticity, 2nd edn*. McGraw-Hill, New York.
Woo SI and Salgado R. (2018). Simulation of penetration of a foundation element in Tresca soil using the generalized interpolation material point method (GIMP). *Computers and Geotechnics*. (94): 106–117.
Zhang DZ, Ma X and Giguere PT. (2011). Material point method enhanced by modified gradient of shape function. *Journal of Computational Physics*. 230(16): 6379–6398.